Resolution enhancement for advanced mask aligner lithography using phase-shifting photomasks

T. Weichelt[1,*], U. Vogler[3], L. Stuerzebecher[1], R. Voelkel[3], U. D. Zeitner[1,2]

[1]*Friedrich-Schiller-Universität Jena, Institute of Applied Physics, Abbe Center of Photonics, D-07743 Jena, Germany*
[2]*Fraunhofer Institute for Applied Optics and Precision Engineering, D-07745 Jena, Germany*
[3]*SUSS MicroOptics SA, CH-2000 Neuchâtel, Switzerland*
***** *tina.weichelt@uni-jena.de*

Abstract: The application of the phase-shift method allows a significant resolution enhancement for proximity lithography in mask aligners. Typically a resolution of 3 µm (half-pitch) at a proximity distance of 30 µm is achieved utilizing binary photomasks. By using an alternating aperture phase shift photomask (AAPSM), a resolution of 1.5 µm (half-pitch) for non-periodic lines and spaces pattern was demonstrated at 30 µm proximity gap. In a second attempt a diffractive photomask design for an elbow pattern having a half-pitch of 1 µm was developed with an iterative design algorithm. The photomask was fabricated by electron-beam lithography and consists of binary amplitude and phase levels.

OCIS codes: (050.1940) Diffraction; (110.3960) Microlithography; (110.5220) Photolithography; (220.4000) Microstructure fabrication; (220.3740) Lithography.

References and links

1. Karl Suss: SUSS Mask Aligner MJB 3 Datasheet.
2. R. Voelkel, U. Vogler, A. Bramati, T. Weichelt, L. Stuerzebecher, U.D. Zeitner, K. Motzek, A. Erdmann, M. Hornung, "Advanced Mask Aligner Lithography (AMALITH)", Proc. SPIE **8326** (2012).
3. L. Stuerzebecher, T. Harzendorf, U.Vogler, U.D. Zeitner, R. Voelkel, "Advanced mask aligner lithography: Fabrication of periodic patterns using pinhole array mask and Talbot effect", Opt. Express **18**, 19485-19494 (2010).
4. L. Stuerzebecher, F. Fuchs, T. Harzendorf, U.D. Zeitner, "Pulse compression grating fabrication by diffractive proximity photolithography", Opt. Lett. **39**, 1042 (2014).
5. S. Bühling, F. Wyrowski, E.-B. Kley, A J M Nellissen, L.Wang, M. Dirkzwager, "Resolution enhanced proximity printing by phase and amplitude modulating masks", J. Micromech. Microeng. **11**, 603 (2001).
6. G.A. Cirino, R.D. Mansano, P. Verdonck, L. Cescato, L.G. Neto, "Diffractive phase-shift lithography photomask operating in proximity printing mode", Opt. Express **18**, 16387-16405 (2010).
7. R. Voelkel, U. Vogler, A. Bich, P. Pernet, K.J. Weible, M. Hornung, R. Zoberbier, E. Cullmann, L. Stuerzebecher, T. Harzendorf, U.D. Zeitner, "Advanced Mask Aligner Lithography: New illumination system", Opt. Express **18**, 20968-20978 (2010).
8. A.K.-K. Wong, "Resolution Enhancement Techniques in Optical Lithography", SPIE Press. Bellingham, Washington, 2001.
9. M.D. Levenson, N.S. Viswanathan, R.A. Simpson, "Improving Resolution in Photolithography with a Phase-Shifting Mask", Electron Devices, IEEE Transactions on **29**, 1828-1836 (1982).
10. M. Fritze, B.M. Tyrell, D.K. Astolfi, R.D.Lambert, D.-R. W. Yost, A.R. Forte, S.G. Cann, B.D.Wheeler, "Subwavelength Optical Lithography with Phase-Shift Photomasks", Lincoln Lab. J. **14**, 237-250 (2003).
11. T. Harzendorf, L. Stuerzebecher, U. Vogler, U.D. Zeitner, R. Voelkel, "Half-tone proximity lithography", Proc. SPIE **7716**, (2010).
12. W.J. Goodman, "Introduction to Fourier Optics", McGraw-Hill, New York, 1968.

13. P.B. Meliorisz, "Simulation of Proximity Printing", Dissertation, Friedrich-Alexander Universität Erlangen-Nürnberg, (2010).
14. K.-H. Brenner, W. Singer, "Light propagation through microlenses: a new simulation method", Appl. Opt. **32**, 4984-4988 (1993).
15. C. Mack, *Fundamental principles of optical lithography* (John Wiley & Sons, 2007), Chap. 1.

1. Introduction

Mask aligner lithography is originally based on shadow printing in order to transfer a photomask pattern into photoresist coated wafers. Mask and wafer can either be in direct contact or in case of proximity lithography separated by an air gap of some 20 to 200 µm. Contact lithography offers a resolution in a range of 0.5 to 1 µm [1], but suffers from contamination and yield problems, as well as a possible damage of the photomask. Residual resist on the mask requires a frequent mask cleaning and shortens its lifetime. Using proximity lithography these problems can be overcome, since it profits from a contact-free exposure process. Furthermore, industrial applications are demanding a high yield, thus proximity lithography is a promising and cost effective alternative to projection lithography, having a comparable high throughput.

However, through the introduction of the proximity gap, the transfer of the mask pattern to the wafer is affected by light diffraction due to the free space propagation from the mask to the wafer. This has a main impact on the quality of the printed features and limits the transferable minimal structure sizes for the case of shadow printing masks. For a proximity distance of 30 µm the resolution is limited to about 3 to 5 µm line width [2].

Recently, it has been successfully demonstrated by Stuerzebecher et al. that it is also possible to fabricate periodic high-resolution structures using a comparable large proximity distance. The proposed approach took advantage of the periodicity of the desired aerial image which simplifies the application of rigorous design algorithm for the mask and benefits from multipole illumination strategies [3,4].

Nonetheless, many applications also require non-periodicity making resolution enhancement for non-periodic structures an exigent issue as well. Some attempts for the generation of high-resolution non-periodic pattern have been made in the past: Bühling et al. designed and fabricated a wave-optically based complex transmission mask. The final photomask did consist of four height levels transforming the phase of light, and two amplitude transmission values. They demonstrated a clear resolution of 3 µm half-pitch for lines and spaces using a proximity gap of 50 µm [5].

Another attempt has been made by Cirino et al. resolving 1.5 µm line width on a resist coated silicon wafer, exposed 50 µm behind the photomask [6]. This approach obtained good lithographic results with a lot of effort by using a photomask on basis of a fused silica substrate covered by an amorphous hydrogenated carbon thin film, acting as amplitude modulation agent. Four additional phase delaying levels were added in order to control the wavefront of the transmitted light.

These first attempts to make use of diffraction effects had to cope with mask aligners with poor mechanical and optical quality as well as less accurate wave-optical simulations. Standard tools lag essential prerequisites like a reliable control of the mask illumination angles what led to results of limited usability in former tries like [5]. Recent developments of mask aligners overcome these drawbacks [7] and make the beneficial use of the phase-shifting technique possible.

The essential degree of freedom for shaping the aerial image and thus improving the resolution is the photomask pattern, while exposure wavelength, proximity distance and the illumination set-up are predetermined by the mask aligner. A beyond that adapted angular spectrum of the illumination helps shaping and improving the final result in the photoresist.

In the current paper we show some new attempts to improve the quality of the transferred pattern while preserving or enhancing the lateral resolution. The attempts make use of the recently developed more reliable mask aligner illumination optics and tries to transfer known principles, like phase-shifting mask structures, from high-resolution projection lithography to shadow printing mask aligner lithography. This is presented in part one of the current paper. In cases where such rather simple modifications are not sufficient to achieve usable printing results an additional wave-optical mask optimization can be applied. The potential of this method is shown in the second part of this paper.

2. Alternating aperture phase shift mask (AAPSM)

Optical lithography research has developed several resolution enhancement techniques, including optical proximity correction, off-axis illumination, and phase-shift photomasks [8]. The aim is to maintain high pattern fidelity at maximum resolution. Phase-shifting photomasks offer the best resolution enhancement potential for sub-wavelength patterning in projection lithography [9,10]. Since projection lithography benefits from the phase-shift method a transfer of this technique to proximity lithography in mask aligner seemed reasonable as the most promising enhancement technique. The method makes use of destructive interference between adjacent pattern by a phase shift of π.

Light that illuminates a conventional binary photomask, as depicted in Fig. 1a) is either reflected (partially absorbed) by the chromium layer (black) or passes the mask through its chromium openings (yellow). The more the feature size on the mask is reduced in size, the more the transmitted light distribution will be affected by diffraction during propagation to the wafer. This will reduce the similarity of the physical light distribution on the wafer and the geometrical shadow of the mask. As a result due to diffraction and interference, areas on the wafer are exposed which are not supposed to be. This is shown in the simulated intensity cross-section at the bottom of Fig. 1a).

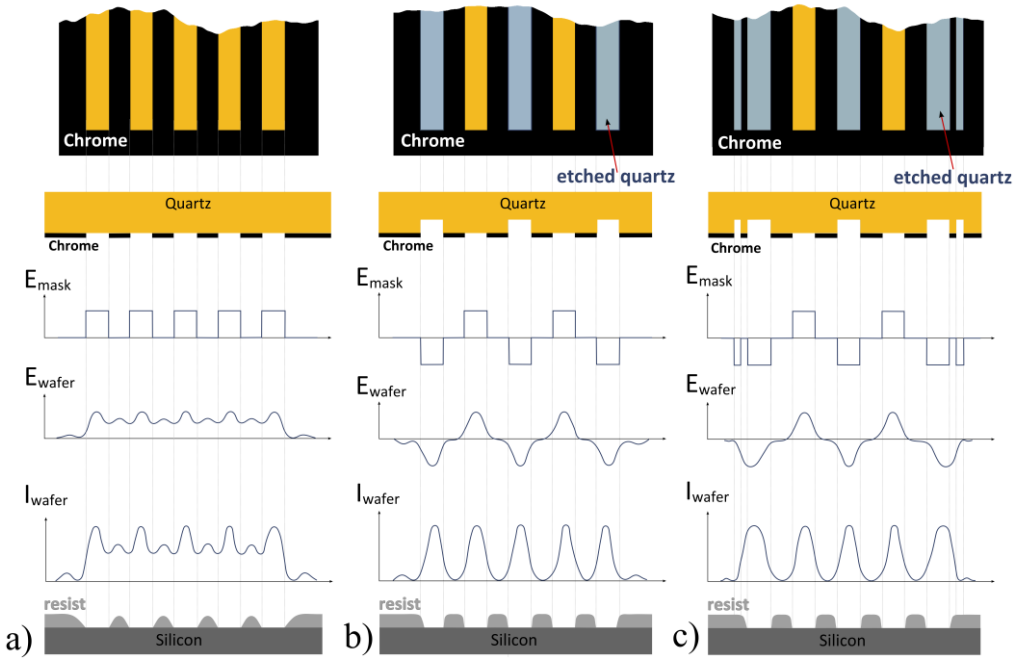

Fig. 1. a) binary amplitude photomask, b) alternating aperture phase-shift mask (AAPSM) and c) AAPSM with additional optical proximity correction (OPC)

For comparison, the function of a mask comprising additional phase shifting structures is sketched in Fig. 1b) and c). The targeted phase shift can be achieved by proper surface structuring of the mask substrate.

Light passing the grooves (blue) experiences different optical path lengths than the light passing the simple binary chromium openings (yellow). Tailored groove depth cause the E-field phase-shifting in comparison to the non-etched regions [9], as it can be seen in Fig. 1b). To obtain a phase-shift of π the depth of the grooves can be calculated using the following relation:

$$\varphi = \frac{2\pi \cdot \left(n_{glass} - n_{air}\right) \cdot d_{PS}}{\lambda}; \qquad (1)$$

not only valid for φ=π. For i-line illumination (λ = 365 nm) and a fused silica mask (n = 1.47) a groove depth of d_{PS}=385 nm is obtained.

Due to destructive interference between waves from adjacent apertures, the exposure intensity (see bottom of Fig. 1b)) is affected and the spatial resolution increased [9]. Additional applied optical proximity correction (OPC) structures (scattering bars) as illustrated in Fig. 1c) can be further used to correct the intensity and hence the width as well as the position of the outer lines of the pattern. These techniques have been used to fabricate structures of 2 µm lines and spaces in 1 µm thick AZ1512 photoresist. Resulting resist pattern are shown in Fig. 2 .

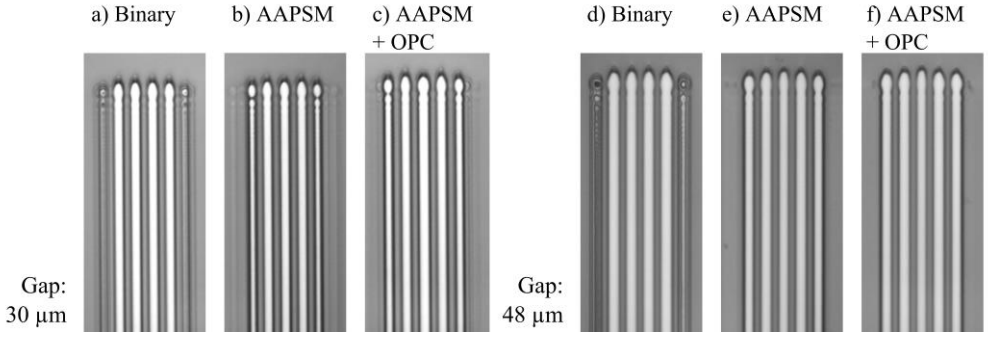

Fig. 2. Microscope images of 2 µm lines and spaces pattern exposed and developed into 1 µm thick AZ 1512 photoresist. Three different photomask designs analog to Fig. 1 have been used and exposed using a proximity gap in the range of 30 µm to 48 µm.

The mask was specified according to the desired line widths and etch depth parameters and purchased from a mask shop. The photolithography process was then made in a SUSS MA6 mask aligner with special illumination optics as described in detail in [7]. By placing special apertures in the light path the illumination angles ν_x/ν_y on the photomask can be defined. In our case, an angular illumination spectrum specified by an illumination filter plate (IFP) as shown in Fig. 3 is applied. This IFP allows a maximum illumination angle of 2°. Illumination wavelength was λ = 365 nm (i-line) and the proximity gap was chosen to be 30 µm. Using a conventional binary mask (Fig. 1a)), a transfer of four instead of the desired five lines into the resist is observed (Fig. 2a)). An alternating aperture phase-

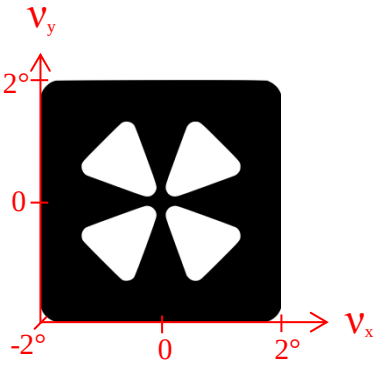

Fig. 3. 45° rotated Maltese Cross - illumination filter plate, generating a specific angular

shifting mask (AAPSM) enables a proper resolution of all five lines, but the outer lines are not exposed similar to the others (Fig. 2b)). The addition of OPC structures of 0.6 µm width and 0.6 µm distance from the outer mask openings can improve the pattern quality significantly, as illustrated in Fig. 2c).

For a stable exposure process a large depth of focus is necessary. Therefore, the depth of focus was exemplarily tested by exposures with different proximity gaps. Fig. 2 shows the start and end of the usable gap range between 30 µm and 48 µm. With the application of the phase-shift method the pattern was resolved satisfyingly for all cases.

Besides a lines and spaces pattern with a pitch of 4 µm an additional pattern with 3 µm pitch (1.5 µm lines and spaces) has been used in the experiments and transferred into the photoresist. Again, the angular spectrum was generated by a 45° rotated Maltese cross IFP, as shown in Fig. 3.

In addition, the experiment has been repeated using an annular IFP (Fig. 4), which was used in combination with a broadband illumination of the full wavelength spectrum of the mercury-arc-lamp of λ≈320…435 nm. This configuration led to the best results achieved for the 1.5 µm half-pitch pattern regarding the equality of the line width and suppression of the undesired artifacts in the photoresist around the pattern, even though the design has been optimized for only one wavelength. Broadband illumination has the advantage of shorter exposure times due to a higher exposure dose.

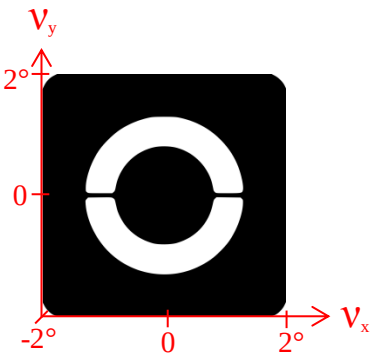

Fig. 4. Annular IFP

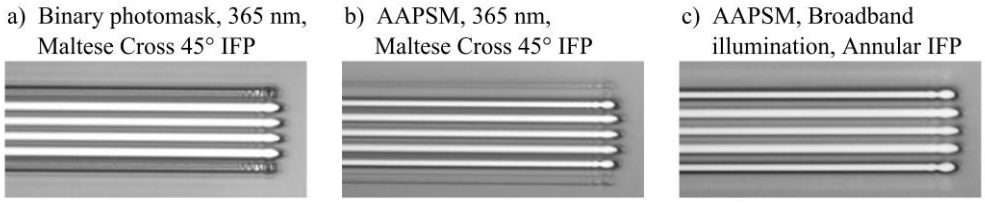

Fig. 5. Photoresist (AZ1512) photographs for 1.5 µm half-pitch lines & spaces (a) binary and (b),(c) alternating phase-shift photomask pattern, in combination with different exposure wavelengths and illumination angle configuration. Proximity distance has been 30 µm.

Figure Fig. 5 a) again shows the pattern of four lines transferred into the photoresist resulting from diffraction at the pure binary mask. The experimental results in Fig. 5b) and c) prove the functionality of the phase-shifting method also for a half-pitch of 1.5 µm.

3. Photomask design by iterative design algorithms

Up to now we have used the additional phase freedom in the mask design only as weak changes to increase the achievable resolution for simple geometries in the proximity printing process.

In a further extension we intend to considerably widen the applicability of this technique to much more complex pattern. As an example for resolution enhancement using diffractive photomasks for we have chosen an elbow pattern consisting of five lines and spaces with different length, shown in Fig. 6 and Fig. 7(a).

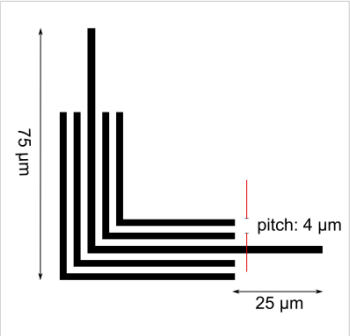

Fig. 6. Elbow pattern with its dimensions.

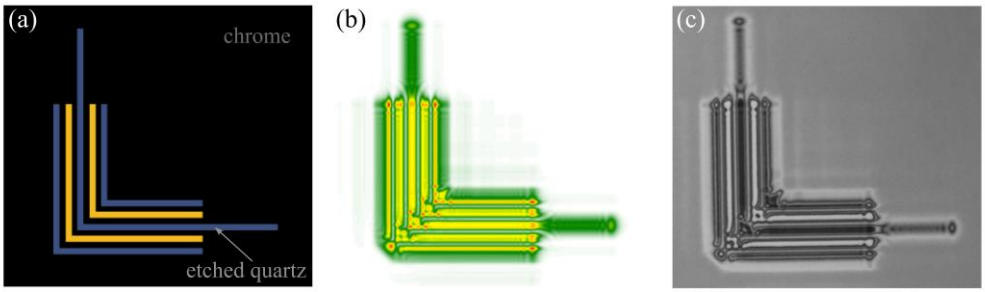

Fig. 7. (a) Transfer of the alternating phase-shift method to an elbow mask pattern design, having a pitch of 4 µm and an outer line length of 50 µm. (b) shows an intensity plot of a simulated aerial image 30 µm behind the mask. The microscope image in (c) shows the exposure results.

In a first attempt the mask was realized by only applying the phase-shift-method as described in section one. As can be seen in Fig. 7 it turned out that for the elbow pattern this is by far not sufficient to obtain acceptable results.

The photoresist micrograph in Fig. 7 (c) illustrates that only two (white) lines have been cleared. In particular, the patterning of the isolated central line is not possible by a simple addition of phase to adjacent lines. Instead, the mask layout has to be designed by a wave-optical method which utilizes the diffraction effects in a well-directed way.

In order to take constraints of the mask fabrication into consideration an iterative design algorithm was applied. It is based on an inverse light propagation between wafer and mask plane. The wafer plane defines the desired exposure intensity distribution which should be copied to the photoresist. The plane directly behind the mask contains a complex field which is given by the wave-optical transmission (amplitude and phase) of the mask geometry. The calculation of the photomask layout is based on back- and forward propagation of the mask transmission and the ideal intensity distribution on the wafer as described in the following. Mathematically, the iteration process is based on projection operators. For this reason, the initial design conditions have a significant impact on the final design the iteration converges to. Hence, a properly chosen initial mask configuration is essential to start the algorithm.

Here, we start the iterative process with a complex photomask illumination given by $U_{-}(x,y,z_M)$. In our case this is a plane wave in normal incidence. After the transmission through the photomask, the distribution can be described as $U_{+}(x,y,z_M) = T[U_{-}(x,y,z_M)]$ where $T[U_{-}(x,y,z_M)]$ denotes the operator describing the mask transmission. This complex field then propagates into the wafer plane.

Due to the fact, that the features of the photomask produce high diffraction angles, a rigorous modeling of the free space propagation is required [11]. The so-called angular

spectrum of plane waves (ASPW) [12] method is applied for the free space propagation along the proximity distance. The resulting aerial image is then given as a complex field $U_+(x,y,z_W)=A(x,y)\cdot e^{i\varphi(x,y)}$.

In the iterative optimization the amplitude distribution of the calculated field is replaced by the target intensity distribution while the phase distribution is kept. After applying these projection operations in the wafer plane the field is then propagated backwards to the photomask plane.

For the transmission of $U_-(x,y,z_M)$ through the photomask a thin element approximation for the mask works best as long as mask feature sizes are significantly larger than the exposure wavelength [13]. Since the minimal feature size of the here described mask pattern is allowed to be smaller than the used illumination wavelength, another method for the transmission calculation was implemented in the design algorithm. The so-called wave-propagation-method (WPM) [14] for finite elements is used for the mask transmission operator to propagate the complex field through the photomask, resulting in $U_+(x,y,z_M)$. The last run of the iteration yields to the quantized amplitude and phase distribution.

In the following flow chart the basic principle of the iterative algorithm is sketched, defining a diffractive optical element as input and the multilevel photomask design as output of the calculation.

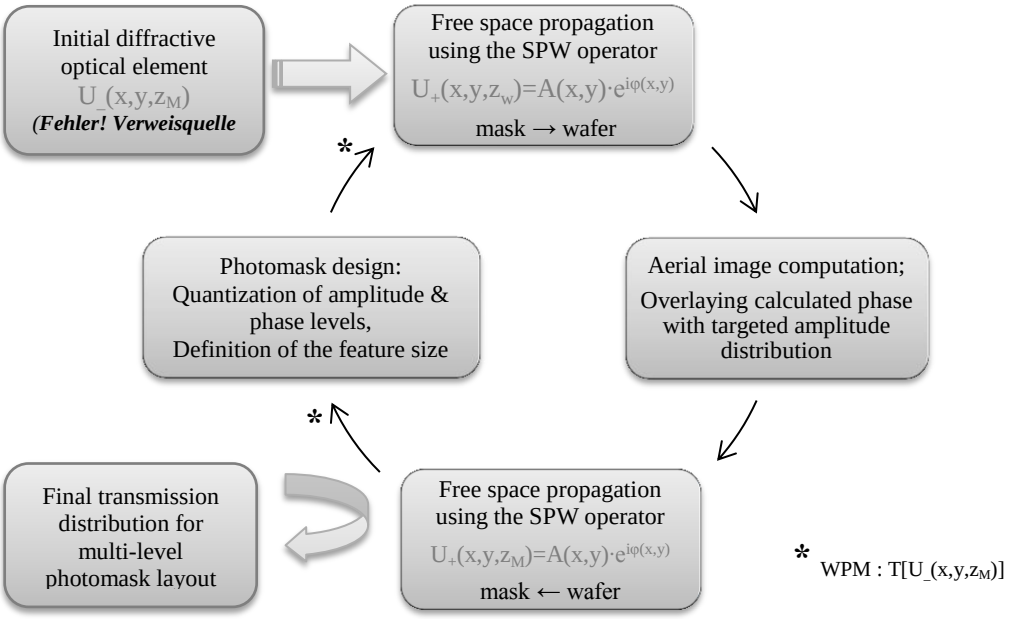

Fig. 8. Flow chart showing the basic principle of the iterative projection algorithm

For the start of the iteration the desired aerial image (Fig. 9) has been propagated back into the mask plane and the resulting complex amplitude distribution was transferred into a mask transmission function using the thin element approximation. This resulting structure is used as the initial diffractive element and is shown in Fig. 10. An alternating phase-shift of adjacent lines has been added as a special feature to the initial phase distribution in the aerial image, visible in Fig. 10 (b).

In order to improve the contrast in the aerial image and steepen the sidewalls of the resist pattern, the target

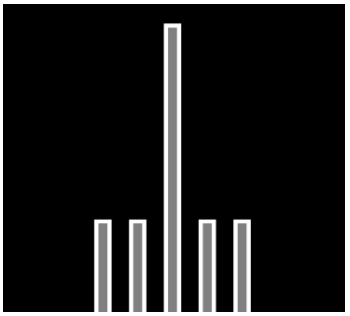

Fig. 9. Clipping of the amplitude distribution defining an amplification of sidewalls of the target pattern

intensity distribution in the wafer plane has been modified by pronouncing the edges of the lines as shown in Fig. 9. This intensity distribution was used in the whole iterative design process as target function.

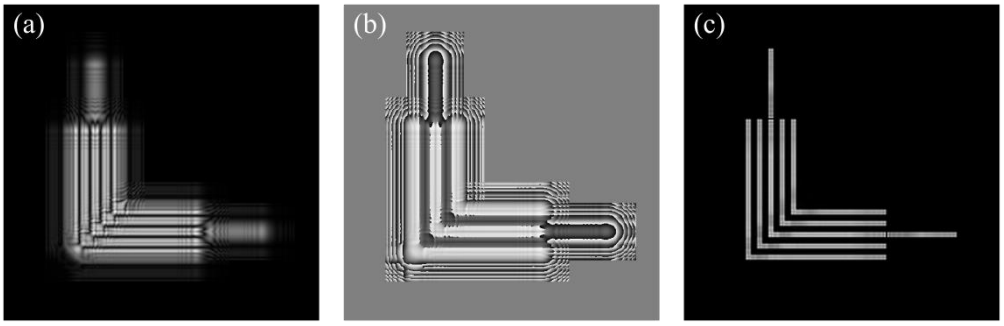

Fig. 10. Initial diffractive element featuring a continuous (a) amplitude and (b) phase distribution providing (c) a perfect intensity distribution as aerial image 30 µm behind the photomask

Such mask designs, like the initial diffractive element, feature continuous amplitude and phase structures which can hardly be fabricated with existing technologies. To enable fabrication, both - amplitude and phase levels – are reduced to a two-levels (or multilevel) design with a minimal feature size of 200 nm which is approximately the limit of our mask fabrication process.

During the photomask design process, the range of amplitude and phase values is reduced stepwise to discrete levels with each additional iteration as a projection operation in the photomask plane. Here also the definition of the minimal feature size with a resampling operator takes place if necessary.

After ten times of back- and forward iteration between mask and wafer plane combined with a stepwise quantization and resampling, the design process results in a diffractive optical element with an aerial image of acceptable quality. The final photomask design contains a binary amplitude- and phase structure, as shown in Fig. 11.

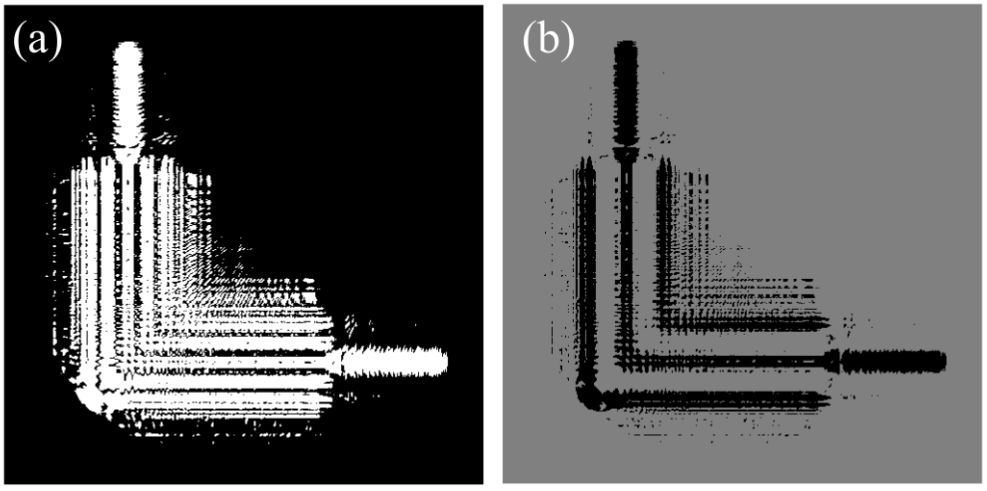

Fig. 11. Resulting mask design after the iterative design algorithm showing the quantized (a) amplitude and (b) phase distribution. An amplitude of one characterizes the chromium openings (white), while a phase of -π (black) means etched grooves into the photomask substrate.

Noticeable is the remaining phase-shift between areas coding the information for adjacent lines of the elbow pattern when evaluating the phase distribution in Fig. 11 (b), which shows the influence and importance of the initial distribution. This resulting mask design yields to a promising aerial image in view of the experimental realization, since the simulated intensity distribution in Fig. 12 shows a suitable quality with good contrast. The aerial image was calculated for the target proximity gap of 30 µm behind the photomask, demonstrating a separation of all five lines, which all have nearly the same width.

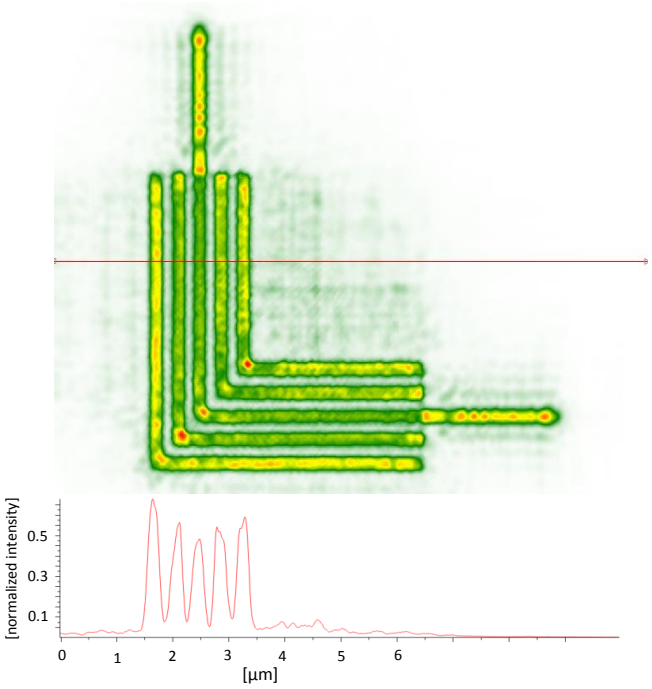

Fig. 12. Simulated intensity distribution of the aerial image, calculated with the iterative design algorithm according to the mask design in figure 11; 30 µm behind the photomask. The red line indicates the position of the shown intensity cross section.

4. Phase-shifting photomask fabrication

The phase-shifting photomask which were used for our experiments have been fabricated using e-beam lithography in combination with a reactive ion etching process.

Two lithography steps were needed to define both - the grooves and the chromium apertures. In the first step the openings for the grooves which are responsible for the phase-shift have been realized. For that, the required pattern was realized first as resist mask by e-beam lithography and transferred into the underlying chromium layer by dry-etching. This chromium structure was then used as a mask for etching the pattern into the fused silica substrate. This guarantees steep sidewalls in the photomask geometry. In a second exposure and the subsequent chromium etching process all additional chromium openings are generated. Figure Fig. 13 shows a scanning electron micrograph of the photomask pattern for the complex elbow layout.

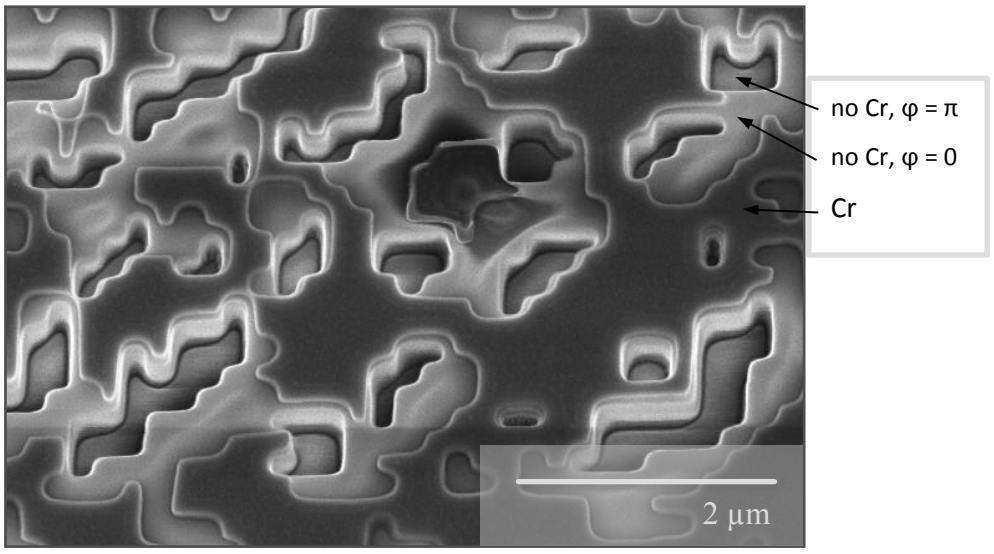

Fig. 13. Scanning electron microscope photograph of the 6" photomask showing the different etched levels of chromium and fused silica to generate the amplitude and phase modulation of the transmitted light.

The chromium layer has a thickness of 96 nm (including 21 nm chromium oxide, standard low-reflective Cr). The surface contains areas where only the chromium is etched away and further areas where additional grooves, with a depth of 385 nm are etched into the fused silica. The depth of the grooves has been specified using the relation of phase-shift and optical path difference in equation (1).

5. Experimental Results

After fabrication of the calculated photomask all so far computed results have been verified by experimental work, realized with a SUSS MicroTec mask aligner of type MA8Gen3 equipped with "MO Exposure Optics" [7].

It turned out that a 45° rotated square as an IFP (Fig. 14) provided the best experimental results. However, even though the pattern is rich in detail, the final results are comparable robust against the change of an IFP.

In the experiments the elbow geometry was exposed in a 500 nm thick AZ1505 photoresist, spin-coated on 4" silicon wafers. The transfer of the pattern was performed applying a 30 µm proximity gap and an exposure dose of 15 mJ/cm^2. Figure Fig. 15 (a) shows a microscope photograph of the resist profile, while (b) shows a scanning electron micrograph of the photoresist profile.

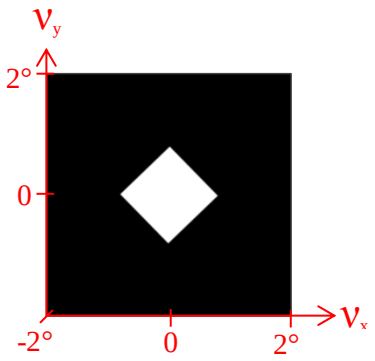

Fig. 14. 45° rotated square as IFP

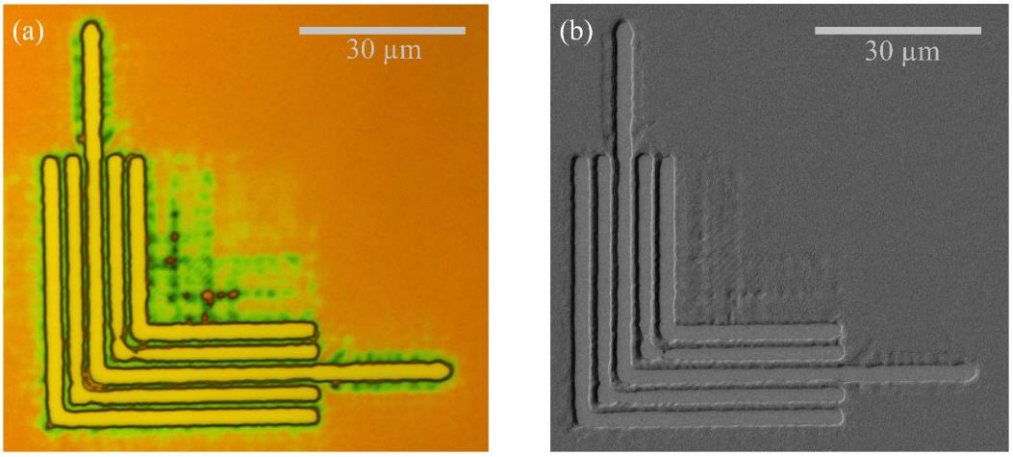

Fig. 15. Photoresist pattern resulting from the mask design presented in figure 11 – (a) visualized in a microscope photograph and (b) as a scanning microscope picture.

The experimental results completely verify the simulation. The generated photoresist pattern resembles its equivalent aerial image in Fig. 15 very well. A resolution of a non-periodic elbow pattern with a half-pitch of 2 µm is successfully demonstrated as the photographs approve. Especially the analogy of simulation and experimental realization has significant importance for further development steps with regard to diffractive mask technology. Hence, the proof of the projection based design algorithm and the validity of using the WPM for the modeling of the light-mask-interaction is ensured, too.

6. Conclusion

With the here presented methods and design algorithms it was possible to fabricate micro structures beyond the classical resolution limit of conventional proximity lithography. The conventional lateral resolution limit is depicted in Fig. 16 and characterized by the equation [15]

$$\Delta x \sim \sqrt{d \cdot \lambda}\ . \tag{2}$$

Assuming a proximity distance of 30 µm a lateral feature size limit of approximately 3.3 µm is determined. From the considered design example the experimentally obtained results approve what has been predicted with the simulation first. By using an additional phase modulation a resolution enhancement was possible. Lateral dimensions of 1.5 µm have been achieved. The red dots in Fig. 16 are indicating the presented pattern resolution with the diffractive photomask.

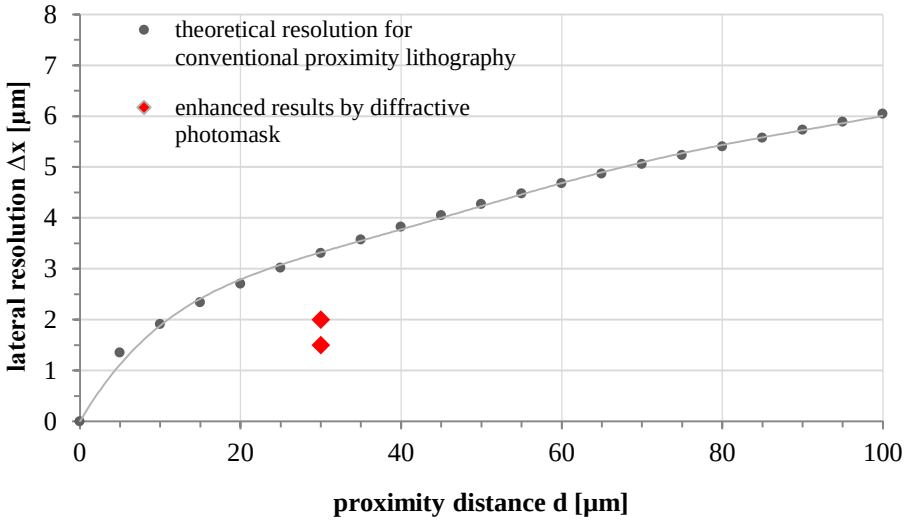

Fig. 16. Lateral resolution as a function of the proximity distance of mask aligner lithography

Conventionally, binary photomasks reach their limit in achievable resolution as the distance between mask and the wafer increase and the structures are supposed to get smaller. The phase-shifting mask significantly helps to overcome this limit. Here, two ways have been shown how it can be adapted to different set of problems.

First, destructive interference between waves from adjacent photomask apertures has been used to reduce diffraction effects and to increase the spatial resolution. In particular, the added phase-shift to a binary photomask enables the resolution of lines and spaces with a half-pitch of 2 µm using a mask to wafer distance of 30 µm. A further improvement of the final photoresist pattern can be achieved by additional OPC structures. As an example, scattering bars correct intensity and hence the width and position of the outer lines of the non-periodic lines and spaces pattern.

For more complex photomask geometries the phase-shift alone is not sufficient for transferring the intended pattern to photoresist properly. An iterative design algorithm based on inverse propagation between mask and wafer helps finding a suitable mask layout for generating the intended photoresist pattern. By combining the phase-shift method and the iterative optimization of the diffractive photomask this concept is extendable to arbitrary pattern geometries.

The final diffractive photomask consisting of a binary amplitude and phase distribution has been realized by e-beam lithography. All simulation results were verified by the experimental realization. The design algorithm in combination with the phase-shift method realized a resolution of a non-periodic elbow pattern having a half-pitch of 2 µm in a proximity distance of 30 µm, therefore beating the conventional resolution limit of proximity lithography by a factor of two. This shows the potential of a further resolution enhancement by using diffractive photomasks in combination with advanced design algorithm.

Acknowledgments

The authors like to thank all colleagues from IOF and IAP photolithography cleanroom team for the reliable photomask fabrication. Furthermore, the authors appreciate the support of Torsten Harzendorf, providing the SEM pictures. The presented results have been partly granted by the German Ministry of Science and Education in the framework of the ultra-optics project “Fertigungstechnologien für hoch entwickelte Mikro und Nanooptiken” (FZK: 03Z1HN32).